PROCEEDINGS OF SCIENCE

Identification of isotopes ^{3}He and ^{4}He with the AMS detector on the International Space Station

Matthew Behlmann* **and Paolo Zuccon**
Massachusetts Institute of Technology (MIT)
Cambridge, MA 02139, USA
E-mail: behlmann@mit.edu

Carlos Delgado and Francesca Giovacchini
Centro de Investigaciones Energéticas, Medioambientales y Tecnológicas (CIEMAT)
E-28040 Madrid, Spain

The isotopic compositions of cosmic ray nuclei are of great interest since they directly reflect processes related to cosmic ray propagation through the Galaxy. In six years of data taking, AMS has collected the largest available data set on fluxes of nuclei. For a selected nuclear charge value, the velocity and rigidity give a measurement of particle mass that allows measurement of relative isotopic abundances. The AMS Ring Imaging Čerenkov (RICH) detector provides particle velocity measurements with resolution better than 0.1%, whereas the silicon tracker provides rigidity determination through the measurement of particle's trajectory in the magnetic field of AMS. In this contribution, we present the methodology used to obtain the isotopic composition of helium nuclei with AMS.

35th International Cosmic Ray Conference — ICRC2017
10–20 July, 2017
Bexco, Busan, Korea

*Speaker.

PoS(ICRC2017)162

1. Introduction & Motivation

1.1 Helium Isotopes in Cosmic Rays

Helium nuclei are the second most abundant component of cosmic rays across a wide range of energies. Previous measurements clearly demonstrate that ^{4}He nuclei, or alpha particles, constitute the majority of this $Z = 2$ flux, with ^{3}He nuclei as a substatntial minority in the rough range 5–25% below 10 GeV/n [1]. These ^{3}He nuclei are deemed secondary cosmic rays, produced by interactions of primary cosmic rays (such as ^{4}He) with the interstellar medium. The relative proportion of helium isotopes within cosmic ray fluxes, or ^{3}He/^{4}He isotope ratio, thus provides valuable insight into the propagation histories of cosmic rays through the Galaxy [2]. Further, the helium cosmic ray flux dwarfs that of all heavier nuclei by an order of magnitude. The Alpha Magnetic Spectrometer (AMS) is well positioned to measure this ratio with unprecedented precision in the energy range from below 1 GeV/n to $\sim$ 10 GeV/n. In this contribution, we present and assess three complementary methods used for measuring ^{3}He/^{4}He in 1×10^8 helium nuclei collected by AMS during 5.5 years of operation.

1.2 The AMS Detector

AMS is a precision, general-purpose magnetic spectrometer designed to identify and measure particles in the GV to TV rigidity range. It is affixed to the International Space Station, where it has taken cosmic ray data continuously since May 2011. AMS is composed of several subdetectors: a transition radiation detector (TRD), four time-of-flight (TOF) scintillator planes, a silicon microstrip tracker, an array of anticoincidence counters (ACC), a ring-imaging Čerenkov (RICH) detector, and an electromagnetic calorimeter (ECAL). A permanent magnet surrounds the inner tracker. Figure 1 shows a cross-section of the detector in the magnet's bending plane. The key

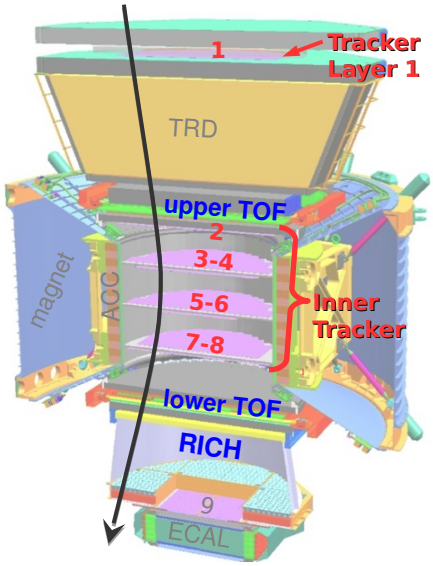

Figure 1: Schematic of the AMS detector with example particle trajectory. The rigidity measurement from the inner tracker is used for this analysis, while TOF and RICH measure velocity. Each highlighted detector component measures charge independently.

components used for isotope identification are the silicon tracker, in conjunction with the permanent magnet; the TOF system; and the RICH detector.

1.3 Measurement of Mass

Mass is measured by combining rigidity ($R \equiv \frac{|p|}{Z}$, for momentum p) and speed ($\beta \equiv \frac{v}{c}$):

$$m = \frac{ZR}{\beta\gamma} \tag{1.1}$$

Gamma represents the Lorentz factor $\gamma \equiv \frac{1}{\sqrt{1-\beta^2}}$. The tracker allows measurement of R, while β is measured by both TOF and RICH. As discussed extensively in the following sections, the AMS resolutions on both R and β prevent us from definitively identifying individual helium nuclei as one isotope or the other. We instead determine the isotope ratio using the totality of events in bins of kinetic energy per nucleon[1], $E_{k/n} = \frac{m}{A}(\gamma - 1)$. In this work, we restrict ourselves to β provided by the RICH because this allows measurement of the isotopic composition in the range 1–10 GeV/n, where existing measurements are sparse and affected by large errors [1].

2. Event Selection

Only downgoing particles within the acceptance of the TOF, tracker layers 1–8, and RICH are relevant for this study. The TOF distinguishes between particles traveling upward and downward through the detector, while the track reconstructed from signals in the tracker indicates the particle's charge sign and whether it impinges on the RICH radiator plane.

A series of independent charge measurments taken along a particle's trajectory allows for a clean selection of events with $|Z| = 2$. Both the inner tracker (layers 2–8) and the two pairs of TOF planes are used, with charge measurement resolution (for $Z = 2$) of $\sigma^Z_{\text{inner}} = 0.07$ and $\sigma^Z_{\text{TOF}} = 0.08$, respectively [3]. A redundant charge selection strategy suppresses events in the tail of measured charge distribution from a single detector, excluding the vast proton flux from our sample.

It is also possible for higher-Z nuclei to undergo fragmentation to $Z = 2$ before reaching the TOF and inner tracker. Tracker layer 1 provides an additional charge measurement to screen out such particles fragmenting in the TRD. Layer 1 charge identification also allows us to quantify fragmentation per amount of material traversed. Applying this rate to the volume above layer 1, combined with the overwhelming abundance of He over heavier nuclei, ensures that the contribution to our sample from fragmentation of nuclei with $Z > 2$ is negligible.

Only galactic cosmic rays (those arriving from outside Earth's magnetosphere) can provide information about propagation through the Galaxy. Thus, it is important to remove particles trapped in Earth's magnetosphere from our sample. For measured speed β, rigidities differ for the two isotopes: $R_4(\beta) > R_3(\beta)$. We require the lower of these, the ^{3}He rigidity R_3, to be above the maximum geomagnetic cutoff rigidity within the AMS field of view [3].

[1] The ratio m/A, mass over number of nucleons, within an approximation of 0.3%, can be considered a constant.

3. Rigidity Measurement with the Silicon Tracker

The tracker consists of nine layers of two-sided silicon microstrip sensors, positioned orthogonally along the vertical axis of the detector. Seven of these, known as the "inner tracker", are located within the magnet bore, where charged particle trajectories bend under the influence of the 0.14 T magnetic field. (See Figure 1.) Each tracker layer measures impinging particle positions in the magnet's bending and non-bending directions with accuracy of approximately 7.5 μm and 30 μm, respectively [3, 4].

The rigidity, R, is obtained from the reconstructed particle trajectory in the AMS magnetic field. The kinetic energy range relevant for this work corresponds to the rigidity range 2 to 25 GV. Such rigidities are best measured using the inner tracker, avoiding the effects of multiple scattering from the detector material between tracker layers 1 and 2 (TRD and upper TOF). Track curvature is proportional to inverse rigidity, which has resolution $\frac{\sigma_{1/R}}{1/R} \approx 10\%$ with a mild dependence on the rigidity itself [4].

4. Velocity Measurement with the RICH Detector

The AMS RICH detector is designed to determine particle velocity with high precision. It consists of a radiator layer with non-overlapping regions of Aerogel and sodium fluoride (NaF) tiles, a detecting plane of photomultiplier tubes (PMTs), and a high-reflectivity conical mirror. The Aerogel and NaF radiators have index of refraction $n = 1.05$ and $n = 1.33$, respectively, giving thresholds $\beta > 0.953$ and $\beta > 0.75$ for production of Čerenkov photons [5]. Correspondingly, the RICH Aerogel (NaF) measurement range is limited to energies above 2.14 GeV/n (0.48 GeV/n).

The opening angle of the Čerenkov light cone, determined from PMT signals and the tracker's reconstruction of particle trajectory at the radiator plane, yields a precise measurement of β. The velocity resolution of the RICH, σ_β, for $Z = 2$ particles is 0.7×10^{-3} (2.4×10^{-3}) for particles passing through the Aerogel (NaF) radiator [5].

5. Methods for Determining Isotope Fraction

The AMS measurement of the particle mass is obtained from R and β using Eq. 1.1. For He isotopes, we expect a peak at 4.002 amu with width ~ 0.4 amu, along with a second peak at 3.016 amu with width ~ 0.3 amu.

The two distributions overlap in large part, impeding event-by-event identification of ^{3}He and ^{4}He isotopes. Yet it is still possible to estimate the overall fraction of each isotope from the measured mass distribution. Herein we present and discuss three methods for the determination of the ^{3}He/^{4}He ratio as function of $E_{k/n}$.

5.1 Analytic Parametrization Based on Rigidity Resolution

Given the large difference between the resolution on R ($\approx 10\%$) and β ($\approx 0.1\%$), the mass resolution is expected to be dominated by the former at low energy. This inverse rigidity has a Gaussian-like distribution. Now consider the inverse mass:

$$\frac{1}{m} = \frac{\beta\gamma}{Z}\frac{1}{R}, \tag{5.1}$$

which should also be Gaussian-like at first approximation. On closer inspection, it becomes apparent that $1/R$ resolution in our measurement range is described by multiple Gaussian forms sharing the same mean, including an asymmetric tail fitted with an asymmetric[2] Gaussian function; Figure 2 shows an example $1/R$ fit. Also note that, even assuming perfect symmetry in $1/R$ and β distributions, the factor $\beta\gamma$ in Eq. 5.1 introduces a slight left-right deformation in the $1/m$ distribution.

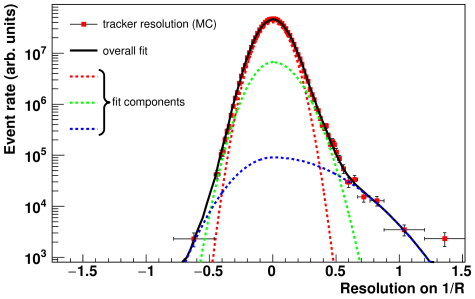

Figure 2: Tracker $1/R$ resolution for $R = 6.5$GV in MC simulation. The solid, black line represents the overall fit ($\chi^2/\text{d.f.} = 68/62$), which is the sum of three components (dotted lines).

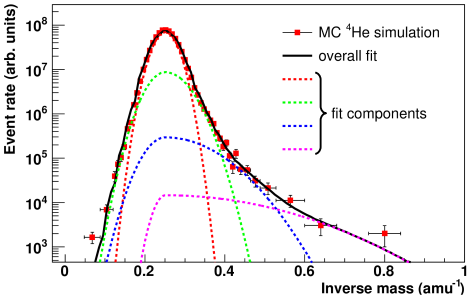

Figure 3: Single isotope ^{4}He inverse mass distribution for $E_{k/n} = 5$ GeV/n from MC simulation with overall fit ($\chi^2/\text{d.f.} = 71.2/53$).

Overall, our analytic function—an sum of Gaussians sharing the same mean with asymmetry as a further degree of freedom—describes the AMS $1/m$ measurement well. Figure 3 shows an example at $E_{k/n} = 5$ GeV/n for only ^{4}He, obtained from a realistic Monte Carlo (MC) simulation of AMS and of the cosmic helium spectrum [3].

With a reliable single-isotope model in hand, it is straightforward to extend this to the two-isotope case. The physics of the two isotopes in the detector are nearly identical, so the two template shapes are closely correlated. The position of the ^{3}He template peak is obtained by multiplying the ^{4}He peak position by the isotope mass ratio. The width parameter of the two templates scales as $\sigma_3/\sigma_4 = \frac{m_4}{m_3}\frac{\sigma_{1/R}(R_3)}{\sigma_{1/R}(R_4)}$; i.e., the isotope mass ratio times a small correction for the fact that ^{3}He and ^{4}He have slightly different rigidities at the same $E_{k/n}$. We extract $\sigma_{1/R}(R_3)/\sigma_{1/R}(R_4)$ from the MC simulation.

The relative normalization of the two isotope templates is left as a free parameter. A fit to data, e.g. Figure 4, yields the isotopic fraction ^{3}He/^{4}He. Agreement of the fitted peak position with $1/m_4$ at the level of 0.1% provides a first validation of our procedure. A second test comes from the evolution of the fitted main Gaussian width as function of the $E_{k/n}$; considering Equation 5.1 with the independence of tracker and RICH resolutions, we have:

$$\frac{\sigma_{1/m}}{1/m} \simeq \sqrt{\left(\frac{\sigma_{1/R}}{1/R}\right)^2 + \left(\gamma^2\frac{\sigma_\beta}{\beta}\right)^2}. \tag{5.2}$$

Fitting this form to $\sigma_{1/m}$ vs. $E_{k/n}$ with a simple linear model for $1/R$ resolution yields $\sigma_\beta/\beta = 7.6 \pm 0.5 \times 10^{-4}$ for the RICH Aerogel regime. This figure matches the resolution measured through other means, providing an additional validation of our method.

[2]The Gaussian width is allowed to take two different values $\sigma_L \neq \sigma_R$ on the left and right sides of the maximum.

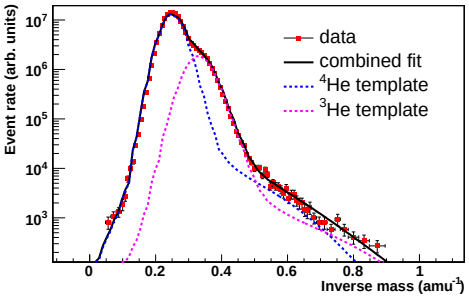

Figure 4: AMS data, $1/m$ distribution for $E_{k/n} = 5$ GeV/n, fitted with two-isotope model (χ^2/d.f. $= 102/89$).

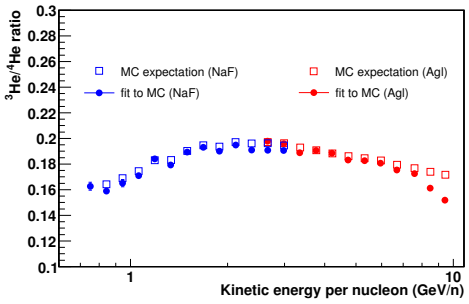

Figure 5: Realistic MC simulation, comparison of the expected values for the ratio (open points) and the fitted one (full points).

The second term under the square root in Equation 5.2 grows rapidly with $E_{k/n}$. Consequently, the hypothesis at the core of our approach becomes more questionable at high $E_{k/n}$. To verify reliability, we implemented a realistic MC simulation incorporating detector response, He spectral shape from [3], and a preliminary isotope ratio measurement. We then applied the same fitting procedure used for the data and compared the result, as shown in Figure 5. As $E_{k/n}$ approaches 10 GeV/n, the fit result is systematically lower than expected. The ratio between fitted and expected is applied to the data measurement as a correction factor, with a corresponding systematic error.

5.2 Data-Driven Templates

It is possible to extract a template for the ^{4}He mass distribution directly from data, taking advantage of Earth's magnetic field shielding effect [6]. The geomagnetic field prevents charged particles with rigidities below the local geomagnetic cutoff, R_{co}, from penetrating Earth's field and reaching AMS. The rigidity cutoff translates into a velocity threshold, β_{co}, which depends on nuclear mass, m:

$$\beta_{co}(m) = \frac{R_{co}Z}{\sqrt{(R_{co}Z)^2 + m^2}} \tag{5.3}$$

This means that when two isotopes of masses $m_{\text{heavy}} > m_{\text{light}}$ arrive with the same velocity, the geomagnetic field may shield the lighter but not the heavier, because $\beta_{co}(m_{\text{light}}) > \beta_{co}(m_{\text{heavy}})$.

For helium isotopes, it is possible to select a sample of cosmic rays with enhanced abundance of ^{4}He for all $E_{k/n}$ bins within our measurement range. Figure 6 shows an example comparison of the helium signal mass distribution with that of events collected between ^{4}He and ^{3}He velocity thresholds for 5.6–6.3 GeV/n. The population of ^{3}He in the latter is heavily suppressed, so we use this sample to build a template for ^{4}He. The residual ^{3}He in the ^{4}He template is mainly due to limited knowledge of the geomagnetic cutoff, and it naturally includes some nuclei that entered AMS as ^{4}He then underwent nuclear interaction to become ^{3}He. A safety margin can be applied to the rigidity cutoff to reduce ^{3}He contamination; however, this should be balanced with other considerations, like statistics and border effects that appear when the sampling region is squeezed toward the cutoff boundary for ^{4}He. The ^{4}He templates extracted from data are also used to verify mass distributions derived from MC.

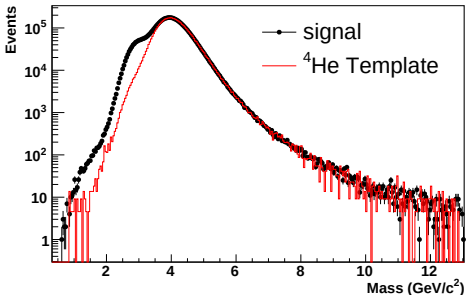

Figure 6: Helium mass distribution in range $5.6\,\mathrm{GeV/n} < E_{k/n} < 6.3\,\mathrm{GeV/n}$ for signal (black points) and ^{4}He template extracted from data (red line).

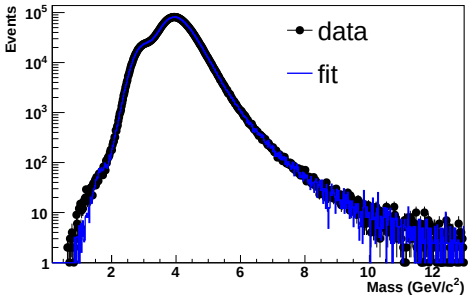

Figure 7: Fit result (blue line) to He mass distribution for energy range $5.6\,\mathrm{GeV/n} < E_{k/n} < 6.3\,\mathrm{GeV/n}$.

The ^{3}He template is obtained by scaling the ^{4}He distribution according to the mass ratio, $\frac{m_3}{m_4}$, under the assumption that the shape is the identical. We use the ^{3}He and ^{4}He templates in a fitting procedure developed to account for residual contamination of ^{3}He on the ^{4}He template. Figure 7 depicts an example fit.

Reliability and systematic effects were tested by fitting ^{3}He and ^{4}He mass distributions from MC simulations to a simulated signal. We determined the maximum amount of ^{3}He contamination in the ^{4}He template that the fitting procedure can handle. In addition, we explored the effects associated with the use of a ^{3}He template derived from the ^{4}He one, instead of an original ^{3}He template, leading to an additional contribution to systematic error.

5.3 Unfolding Method

Our best knowledge of the response of the detector is parameterized in its response matrix. Given the measured inner tracker momentum distribution for a given β bin, the distribution of true momentum can be obtained using an unfolding method and the migration matrix. This method has the advantage of automatically accounting for all effects included in the migration matrix, including detection efficiencies and interactions, to provide the ratio at the top of the detector.

The method proceeds by building the tracker migration matrix from an MC simulation sample and smoothing statistical fluctuations in each true momentum bin. The normalization of the migration matrix is chosen to reflect the acceptance of our analysis. Then the data sample is split by measured β, in bins smaller than RICH resolution. For each one of these bins, the measured momentum distribution is unfolded using an Expectation–Maximization algorithm [7], regularized by imposing that the unfolded distribution should be compatible with two peaks of the expected width, as explained below. The ^{3}He/^{4}He result is the ratio of events under each of these peaks.

Under suitable conditions, the expected width of each peak is

$$\frac{\sigma(R)}{R} = \gamma^2 \frac{\sigma(\beta)}{\beta}, \tag{5.4}$$

where the β is given by the mass of the isotope and the mean of the unfolded momentum. These conditions come from the necessity to have a nearly monochromatic momentum sample in the selected β bin. We require that:

(a) the measured β bin be finer than σ_β;

(b) $\frac{\partial \sigma_\beta}{\partial \beta}$ be much smaller than σ_β; and

(c) $\frac{\partial N}{\partial \beta}$ be much smaller than $N(\beta)$, where $N(\beta)$ is the differential spectrum in β.

Condition (a) is fulfilled by choosing appropriate bins, (b) is true for the RICH resolution, and (c) is fulfilled for the typical cosmic ray flux if β is sufficiently far from 1.

Once a β bin has been unfolded, we perform a cross-check in two parts. First we fold the result with the migration matrix and compare with the measured momentum distribution to verify that the regularization hypotheses are correct. Then we compare the positions of the resulting peaks with the masses of the two isotopes. These checks allow us to assess the energy range where the method is valid. Finally, the ratio of normalizations of the two peaks provides the ratio of abundances of the isotopes already corrected by all effects described in the MC.

Figure 8 shows the result of the unfolding for a single fine bin, wherein the peaks are clearly separated. Figure 9 shows the fit of the folded result to the data. We can see that the regularized, unfolded peaks correctly describe the data.

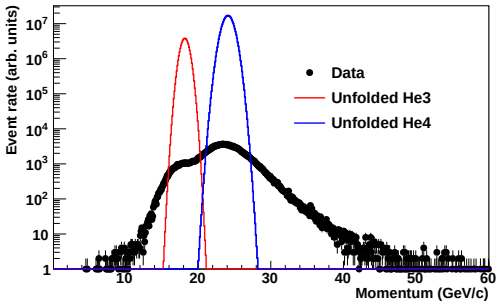

Figure 8: Unfolded momentum distributions for events near $E_{k/n} = 5$ GeV/n compared with measured momentum for those events. Unfolded distributions are multiplied by an arbitrary factor for plotting on the same axes.

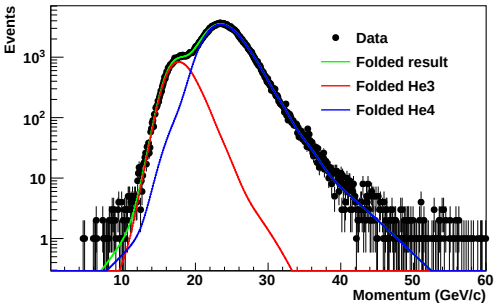

Figure 9: Re-folding of the distributions shown at left, along with their sum (in green), for comparison with data in $E_{k/n} = 5$ GeV/n bin.

The main systematics intrinsic to this method are given by the knowledge of the tracker migration matrix and knowledge of β resolution. The former has been deeply studied for the measurement of the helium flux [3], and agreement with data has been confirmed directly using data selected with the RICH at sufficiently low γ. For the latter, at $\beta = 1$ the RICH resolution is measured directly. Both a flat β dependence and the β dependence obtained from MC simulation are considered.

6. Conclusions

We present three diverse and complementary approaches to the measurement the flux ratio ^{3}He/^{4}He using tracker, RICH, and TOF. Each method makes use of extensive studies of detector properties and resolution, as well as the information from Monte Carlo simulation. Complementarity of methods and systematics provides a robust validation of our result.

References

[1] M. Aguilar *et al.*, *Isotopic composition of light nuclei in cosmic rays: results from AMS-01*, *Astrophys. J.*, **736** (2011), 105.

O. Adriani *et al.*, *Measurements of cosmic-ray hydrogen and helium isotopes with the PAMELA experiment*, *Astrophys. J.*, **818** (2016), 68. arXiv:1512.06535 [astro-ph].

Z. D. Myers *et al.*, *Cosmic Ray ^{3}He and ^{4}He Spectra from BESS 98*, in proceedings of the 28th ICRC (2003).

O. Reimer, *et al.*, *The Cosmic-Ray ^{3}He/^{4}He Ratio from 200 MeV per Nucleon^{-1} to 3.7 GeV per Nucleon^{-1}*, *Astrophys. J.*, **496** (1998), 490.

[2] N. Tomassetti, *Propagation of H and He cosmic ray isotopes in the Galaxy: astrophysical and nuclear uncertainties*, *Astrophys. Space Sci.*, **342** (2012), 131. arXiv:1210.7355 [astro-ph].

[3] M. Aguilar *et al.* (AMS Collaboration), *Precision Measurement of the Helium Flux in Primary Cosmic Rays of Rigidities 1.9 GV to 3 TV with the Alpha Magnetic Spectrometer on the International Space Station*, *Phys. Rev. Lett.*, **115** (2015), 211101.

[4] G. Ambrosi *et al.*, *AMS-02 Track reconstruction and rigidity measurement*, in proceedings of the 33rd ICRC (2013).

[5] H. Liu *et al.*, *The RICH detector of AMS-02: 5 years of operation in space*, *Nucl. Instr. Meth. Phys. Res. A* (in press).

[6] W. Gillard, F.Barao, L.Derome, *Isotopic Identification with the Geomagnetic Field for Space Experiments*, in proceedings of the 32nd ICRC (2011).

[7] A.P. Dempster, N.M. Laird, D.B. Rubin, *Maximum Likelihood from Incomplete Data via the EM Algorithm*, *J. Royal Stat. Soc., Series B*, **39** (1977), 1.